Real-time visualization of intracellular hydrodynamics in single living cells

Eric O. Potma*, Wim P. de Boeij*, Peter J. M. van Haastert†, and Douwe A. Wiersma*‡

*Ultrafast Laser and Spectroscopy Laboratory, Materials Science Centre, and †Groningen Biomolecular Sciences and Biotechnology Institute, University of Groningen, Nijenborgh 4, 9747 AG Groningen, The Netherlands

Communicated by Mostafa A. El-Sayed, Georgia Institute of Technology, Atlanta, GA, December 5, 2000 (received for review July 11, 2000)

Intracellular water concentrations in single living cells were visualized by nonlinear coherent anti-Stokes Raman scattering (CARS) microscopy. In combination with isotopic exchange measurements, CARS microscopy allowed the real-time observation of transient intracellular hydrodynamics at a high spatial resolution. Studies of the hydrodynamics in the microorganism *Dictyostelium discoideum* indicated the presence of a microscopic region near the plasma membrane where the mobility of water molecules is severely restricted. Modeling the transient hydrodynamics eventuated in the determination of cell-specific cytosolic diffusion and plasma membrane permeability constants. Our experiments demonstrate that CARS microscopy offers an invaluable tool for probing single-cell water dynamics.

Water is the major molecular constituent of a cell, comprising about 70% of its average weight (1). Unlike many other intracellular constituents, water easily migrates over the plasma membrane and rapidly exchanges between intra- and extracellular domains (2). Cellular hydrodynamics is affected by details of the chemical composition of the cytosol as well as by structured water shells, which encompass macromolecular intracellular structures. The joint effects of semipermeable membrane barriers and the local properties of the aqueous cytoplasm ultimately determine intra- and extracellular water dynamics (3). Because water provides the dynamical matrix in which all biochemical and biophysical processes occur, knowledge of intracellular hydrodynamics is of vital importance to understanding the functioning of living cells.

Measurement of water membrane permeability as well as intracellular water diffusion in living cells is far from trivial. Although the osmotic membrane permeability constant (P_f) can be obtained by monitoring the cell volume change on changing osmotic conditions, the diffusion permeability constant (P_d) of biological membranes is more difficult to access (2). Indirect fluorescence techniques and NMR methods have been used to determine P_d in a variety of cell types (4–6). Information on intracellular water diffusion coefficients (D_w) in biological systems has been provided mainly by NMR measurements (7, 8). Although MRI techniques allow the determination of water diffusion coefficients in biological tissues, restrictions in spatial resolution make NMR techniques less suitable for exploring water mobility in a single living cell.

In this paper, we report on an all-optical microscopic registration method of dynamical water distributions in living cells. The method is based on vibrational contrast in a coherent anti-Stokes Raman scattering (CARS) laser-scanning microscope (9–11). Similar to conventional Raman methods, CARS vibrational spectra uniquely characterize biological (macro-) molecules in condensed phase systems and thus provide a direct means to selectively probe specific chemical species (12, 13). The contrast in CARS microscopy results from vibrational active modes of molecular compounds and does not rely on complicated and possible interfering staining procedures commonly used in fluorescence microscopy.

Whereas earlier methodologies of the CARS technique were not optimized for live cell studies (9), the point-like illumination method recently proposed by Zumbusch *et al.* allows CARS imaging on living cellular systems with high three-dimensional resolution (10). In combining subpicosecond excitation with a collinear excitation scheme, it was shown that regions rich in aliphatic C–H vibrations can be visualized successfully in live cells by using a CARS microscope. One of the keys to this success is that the background CARS signal from water can be sufficiently suppressed.

Here, we focus on this CARS signal from water and use it as a probe for intracellular hydrodynamics. By using the point-illumination method, the exceptionally high resonant signal yields obtained from water give rise to data acquisition times that enable real-time vibrational imaging of live cells. We show that spatiotemporal hydrodynamics in single living cells can be followed in real time in a CARS microscope, by monitoring the transient intracellular H_2O/D_2O exchange. The high contrast obtained in the advanced CARS microscope in combination with high three-dimensional spatial resolution enables a clear recording of spatially varying diffusion patterns in live cells. The diffusion permeability of the plasma membrane and the intracellular water diffusion coefficient can be readily extracted from these effusion experiments.

BIOPHYSICS

Materials and Methods

CARS microscopy is a multicolor technique that requires a pump beam, a redshifted Stokes beam, and a probe beam. The degenerate pump–probe beam is derived from a home-built femtosecond visible optical parametric oscillator (OPO) (14), tunable between 570 and 670 nm, that is pumped by the second harmonic of a Ti:sapphire laser (Tsunami, Spectra-Physics). The remainder of the pumping 800-nm radiation is used as the Stokes beam in the experiment. An acoustic-optical modulator is inserted into one of the arms of the OPO for providing cavity dumping. CARS experiments are conducted at a dumping frequency of 800 kHz. To synchronize both beams, the infrared radiation is pulse picked at the same rate by slaving a second Bragg cell driver to the dumper unit of the OPO. A prism compressor is introduced in the optical paths of both beams to minimize the temporal width of the pulses at the sample position.

The visible pump–probe pulses are variably delayed by a computer-controlled delay stage to assure temporal overlap with the Stokes beam. The beams are spatially filtered, expanded by telescope, and collinearly combined on a dichroic mirror. After the beams have passed a pair of scanning mirrors (Cambridge Technology, Cambridge, MA, no. 6860) and a scan lens, they are coupled into an inverted microscope (Zeiss Axiovert S100 TV) and focused onto the sample by an objective lens. The radiation

Abbreviations: CARS, coherent anti-Stokes Raman scattering; OPO, optical parametric oscillator; ANTS, aminonaphtalene-trisulfonic acid; TPE, two-photon excited.

‡To whom reprint requests should be addressed. E-mail: wiersma@chem.rug.nl.

The publication costs of this article were defrayed in part by page charge payment. This article must therefore be hereby marked "*advertisement*" in accordance with 18 U.S.C. §1734 solely to indicate this fact.

Article published online before print: *Proc. Natl. Acad. Sci. USA*, 10.1073/pnas.031575698. Article and publication date are at www.pnas.org/cgi/doi/10.1073/pnas.031575698

is recollimated by a second objective in the forward (transmission) direction. A microscope objective of ×40, 0.75 numerical aperture (n.a.) (Zeiss Plan Neofluar) is used for excitation, whereas a ×20, 0.5 n.a. (Zeiss C-Apochromat) objective was used for collimation. The lower magnification of the collimating objective was chosen because of the larger working distance of the lens, which allows the insertion of a perfusion chamber at the sample position. CARS signals are separated from the excitation light by means of a bandpass filter (Omega Optical, Brattleboro, VT) and detected by a photomultiplier (Hamamatsu Phototonics, Hamamatsu City, Japan, no. R5600U-04). A stepper motor provides scanning in the axial direction. In all of the imaging experiments, the average powers were kept below 100 μW per beam to ensure minimal thermal and photoinduced damage to the cells. Note that the coherent nature of the CARS signal is reflected in the square dependence of the signal intensity on the probe concentration.

For typical settings used in the experiment, about 500 signal photons per laser shot are detected, meaning that data acquisition times are limited by instrument response time (beam-scanning rate) rather than by photon statistics (data-collection time per pixel). The spatial resolution resembles that of a conventional confocal microscope and amounts to 0.36 μm in the lateral dimension and 2.0 μm in the axial direction.

CARS spectra were obtained by tuning the visible pump–probe beam while keeping the Stokes beam fixed at 800 nm. To detect the spectrally varying CARS signal, a double monochromator (Spex Industries, Metuchen, NJ) was used instead of spectral filters. Although the visible beam was spectrally tuned, the average power at the sample was kept constant. Because of the broad tuning range, the time delay between the beams was adjusted to compensate for variations in temporal overlap induced by dispersion effects. Raman spectra were taken by illuminating aqueous solutions with the 488-nm line from an Argon ion laser. The scattered light was spectrally resolved by a triple spectrometer (Spex) and detected by a optical multichannel analyzer (Princeton Instruments, Trenton, NJ).

Two-photon excited (TPE) fluorescence is detected in the epi direction (15). Signals were separated from the excitation light by a dichroic mirror (Chroma Technology, Brattleboro, VT). Colored glass filters (nos. BG25 and BG39, Schott, Mainz, Germany) are used to eliminate any remaining radiation of the laser beams at the position of the photomultiplier (Hamamatsu R5600P-01, selected for single-photon counting). Fluorescence lifetimes were determined by using time-gated detection (16). In brief, single-photon-counting electronics were used to count the number of photons in either of two consecutive time windows of 5 ns and 20 ns, respectively, that were triggered by the excitation pulse. Assuming an exponential decaying population of the fluorescent state, the fluorescence lifetime can be determined from the balanced ratio of the intensities of the two channels.

Spatiotemporal traces as obtained from water efflux experiments were subjected to a correlative image analysis procedure by using the program IMAGIC on a Silicon Graphics (Mountain View, CA) workstation. Individual traces were scaled to the average cell width and subsequently averaged.

Intracellular hydrodynamics were studied in *Dictyostelium discoideum* amoebae. *D. discoideum* wild-type strain AX3 cells, and aquaporin-transformed act15::rd28 cells were cultured in HG5 growth medium. Before the experiments, cells were rinsed twice with a phosphate buffer (10 mM, pH 6.4) and brought into a perfusion chamber. The fluophore aminonaphtalene-trisulfonic acid (ANTS, Molecular Probes) was used in the fluorescence lifetime experiments. *D. discoideum* cells were labeled with this fluophore by incubating the cells for 30 min in a 10-mM buffered solution of ANTS (pH 6.4). All experiments were conducted at room temperature. Cell viability was checked by inspecting the cells after the water efflux experiments.

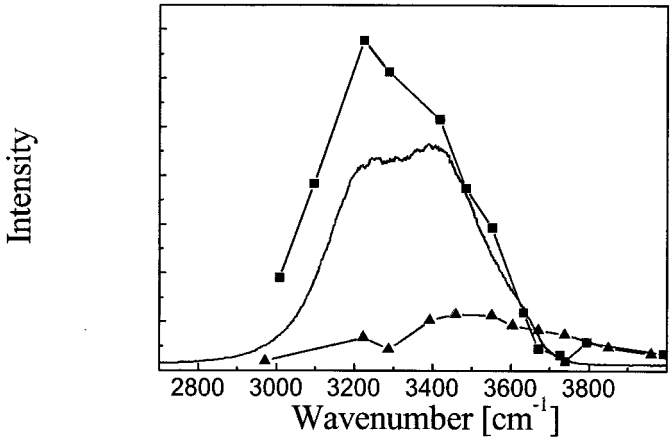

Fig. 1. Vibrational spectra in the region of the O—H stretch vibration of water. Squares correspond to CARS spectrum of distilled water, whereas triangles refer to the CARS response from D_2O. The solid line represents the spontaneous Raman band profile.

Dictyostelium cells resumed migrating activities within 10 minutes subsequent to several imaging sessions.

African green monkey kidney (COS-1) cells were cultured on coverglasses immersed in 90% Dulbecco's MEM and 10% FBS. Coverglasses were mounted into the perfusion chamber, and cells were allowed to adjust to room temperature for 1 hour. The duration of the imaging sessions was minimized to less then 1 hour per glass slide.

Results and Discussion

Imaging of Individual Cells. The isolated O—H-stretching mode of water centered at 3,300 cm^{-1} is addressed in the laser experiment and used as a probe for water concentration. As depicted in Fig. 1, the CARS spectrum agrees with the Raman band profile. The characteristic dispersive lineshape of the CARS spectrum (12) can be recognized in the figure. No resonant contribution is observed from the O—D-stretch vibration of heavy water (deuterium oxide, D_2O) in this region, permitting the use of D_2O as a contrast agent to resolve the transient distributions of intracellular water. As a result of the isotope effect, the position of the O—D-stretch vibration is shifted down to 2,800 cm^{-1}, out of resonance with the laser beams. Despite the intrinsic broad bandwidth of the femtosecond laser radiation, isolated vibrational lines like the O—H-stretch vibrations are still uniquely addressed with this technique. To visualize water distributions exclusively, the OPO was tuned to 636 nm, corresponding to a center frequency of 3,220 cm^{-1}.

The water content in living *D. discoideum* cells can be recognized easily in a CARS image (Fig. 2*a*). Signal levels derived from the aqueous compartments of the cell compare with the signal intensities measured in the extracellular environment. Contrast in the CARS image is raised by hydrophobic and highly scattering regions like the plasma membrane, as well as intracellular structures that show up as dark regions in the CARS image. The morphology of the cell as deduced from the CARS recording is confirmed by a simultaneously recorded TPE autofluorescence image (Fig. 2*b*). Distinct intracellular organelles can be recognized in both images.

Monitoring Intracellular H_2O/D_2O Exchange. Vegetative *D. discoideum* cells were incubated in a perfusion chamber that was initially filled with aqueous phosphate buffer solution at room temperature. Cells were allowed to tightly adhere to the glass slide. At a given moment, the perfusion chamber was rapidly flushed with an isotonic D_2O buffer solution. During the process

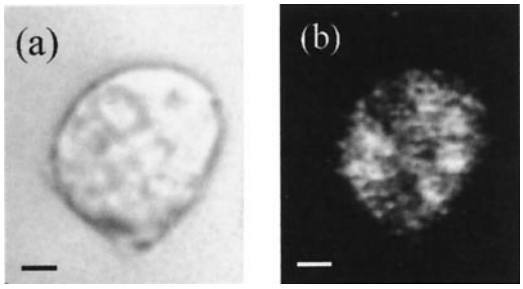

Fig. 2. Coherent anti-Stokes Raman scattering microscopy of *D. discoideum*. (*a*) CARS image of a single dictyostelium cell in aqueous medium. Pump laser was tuned to 636 nm, and Stokes beam was set to 800 nm to address the O—H-stretch vibration of water. The image is recorded in 5 s and consists of 16 averages per pixel. (Bar = 2 μm.) (*b*) Autofluorescence image measured simultaneously with *a*.

of H_2O/D_2O exchange, the interior and exterior of a single cell were imaged by repetitive scanning of the focal spot along a line parallel to the equatorial axis of the cell at a height $\approx$1 μm above the glass surface. While the signal that was measured in the extracellular domain drops with a time constant dictated by the response time of the perfusion chamber ($\tau \approx 1.5$ s), the interior domain of the cell shows a significantly slower response, as shown in Fig. 3. While the diffusion process affects the water concentration in the intracellular compartment of the cell, the extracellular flow is maintained to prevent the buildup of an external unstirred layer. It is known that this effect would lead to erroneous predictions in permeability and diffusion (2). In transient imaging experiments, *D. discoideum* cells adopt a semispherical shape as a consequence of the mechanical stress induced by the shear force during the flushing process.

Because the efflux rate is characterized by the permeability P_d of the plasma membrane and an effective diffusion coefficient D_w assigned to the intracellular space, examination of the measured spatiotemporal trace may eventuate directly in the determination of both coefficients. Given the square dependence of the CARS signal to the concentration of the probe species, the change in CARS signal intensity directly translates to changes in local water concentration at a given time. Measurements were repeated for various H_2O to D_2O and D_2O to H_2O exchanges, whereby no apparent differences were observed in the applied sequence. We have hereby assumed that the diffusion and permeability constants of H_2O and D_2O are the same. The response of *Dictyostelium* cells to heavy water solutions was checked by incubating cells in D_2O buffer. The cells were able to survive in D_2O medium for many hours, retaining their original morphology.

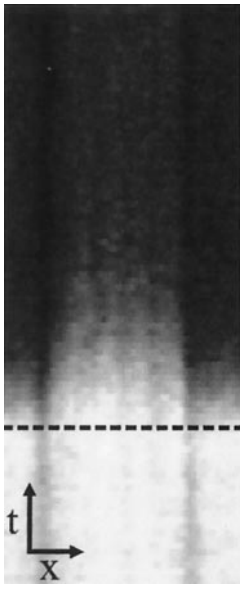

Fig. 3. Spatiotemporal CARS recording of a single cell that is initially immersed in aqueous medium and subsequently flushed with isotonic D_2O medium. The dashed line indicates the moment at which the perfusion chamber is flushed. Shaded horizontal lines correspond to the position of the plasma membrane. Arrows, 3 μm (horizontal, x), 1.5 s (vertical, t).

Intracellular Water Diffusion. The capability of addressing water molecules in the CARS experiment provides a direct means to measure local water concentrations and opens the way to supplement temporal information with transient features in the spatial dimension. This virtue is exemplified in recordings of equatorial scans in single *D. discoideum* cells (Fig. 3), where a significant spatial modulation during the rapid exchange of H_2O with D_2O molecules can be discerned. In Fig. 4*a*, recordings of 24 independent measurements on different cells were averaged. Individual traces were corrected for intensity variations, as induced by scattering at the plasma membrane and intracellular structures. The resulting pattern of the transient intracellular water concentration shows that the interior of the cell can be divided spatially into two regions with different diffusion properties. At a given time during H_2O/D_2O exchange, the H_2O concentration profile in the central region of the cell is nearly spatially invariant, whereas in the zone near the cell border, the H_2O concentration rapidly decreases toward the plasma membrane. Experimental traces are simulated by a diffusion model that assumes a high-average diffusion coefficient throughout the whole intracellular space, except for the region near the cell membrane where D_w is significantly smaller (see *Appendix*). On the basis of this model, the layer with restricted water mobility along the plasma membrane is characterized by a width of 10–20% of the cell diameter and a diffusion constant of $D_w \approx 5$ $\mu m^2/s$. Such extremely low water diffusion coefficients are generally attributed to hydrated water structures and have been observed, for instance, in neuronal fibers in rat brains and in gels of dextran (17, 18). In contrast, the mobility of water molecules in the central region of the cell is not severely restricted and resembles the motional properties of water in aqueous buffer solutions ($D_w > 500$ $\mu m^2/s$). The exceptionally low D_w in the vicinity of the plasma membrane may be ascribed to the presence of densely packed actin filaments in this region that provide an additional barrier in the process of water diffusion. It is known that either mechanical or osmotic stress induces a redistribution of actin in the peripheral parts of the cell (19, 20).

Membrane Permeability. The distribution of plasma membrane permeability coefficients as derived from fits to the experimental data is given in Fig. 5. A mean value of $P_d = 2.2$ μm/s is found with a standard deviation of 0.7 μm/s, indicating that the cell-to-cell variation is relatively small. Compared with the well-studied membrane permeability of erythrocytes ($P_d \approx 50$ μm/s) (2), the observed membrane permeability of *D. discoideum* is rather low. The high membrane permeability of erythrocytes is explained in terms of the composition of the lipid bilayer, including the presence of water channel proteins. The permeability of *D. discoideum* cells corresponds to a lipid composition of the plasma membrane (21) without water channels. It was recently reported that the *wacA* gene encoding for a water transport membrane protein is probably not expressed in vegetative amoebae of *D. discoideum* (22).

We have repeated these experiments with *D. discoideum* cells

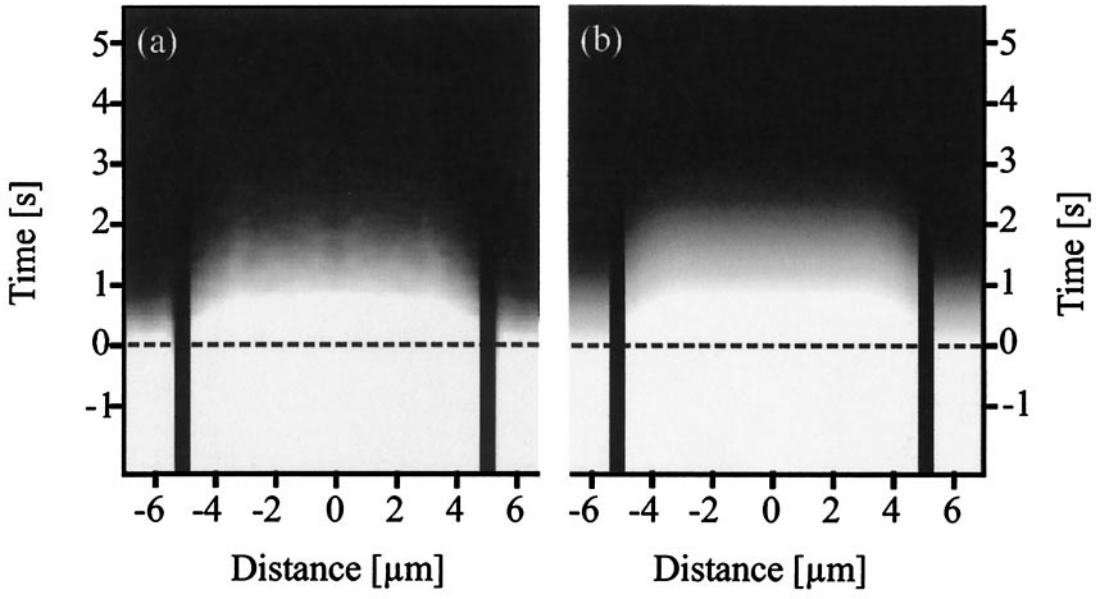

Fig. 4. Comparison between experimental traces and simulation. (*a*) Experimentally determined water concentration profile in a single *D. discoideum* cell. Medium exchange starts at $t = 0$, indicated by dashed line. Vertical black lines mark the positions of the plasma membrane. Figure was corrected for variations in signal because of scattering at membranes and intracellular structures. The image is composed from the average of 24 individual measurements by correlative image analysis; the *x* axis is scaled proportional to the average cell diameter. (*b*) Simulation based on the model of a spatially dependent diffusion coefficient. The region of restricted water diffusion adjacent to the plasma membrane is set to 20% of the cell diameter. A diffusion constant of $D_w = 5\ \mu m^2/s$ was used in the simulation for the zone of restricted water diffusion; outside this region, the diffusion was assumed to be water-like ($D_w > 500\ \mu m^2/s$). The membrane permeability was found to be $P_d = 2.2\ \mu m/s$.

that were transformed with a construct encoding for a water channel protein (aquaporin, *Arabidopsis thaliana*) (23). The transformed cells exhibit an increased permeability of the plasma membrane. As can be seen in Fig. 5, a significant fraction of the measured cell population has a larger membrane permeability, which is ascribed to the incorporation of active aquaporins into the cellular plasma membrane.

Comparable CARS experiments on COS cells at room temperature yield a mean permeability coefficient of $P_d = 38\ \mu m/s$. The water efflux in the COS cells is more than one order of magnitude faster than in AX3 *D. discoideum* and underlines the remarkably low membrane permeability of the latter. In COS cells, no regions of restricted water diffusion could be identified within the spatial and temporal limits of the experiment.

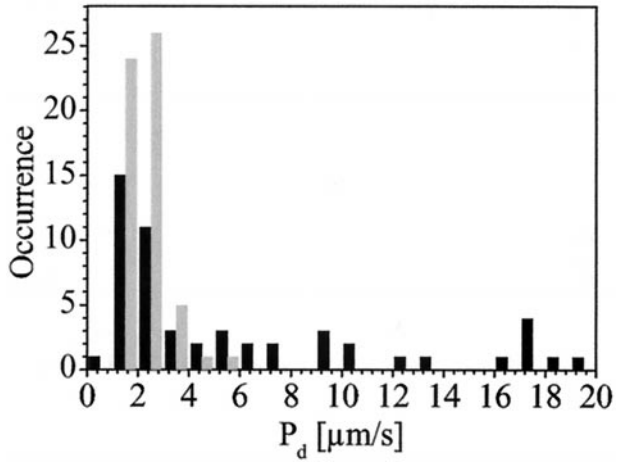

Fig. 5. Analysis of plasma membrane permeability as determined from water efflux measurements. Distribution of membrane permeability constants of AX3 *D. discoideum* cells (gray bars) and of aquaporin-transformed act15::rd28 cells (black bars).

Comparison with Fluorescence Methods. Unlike more established methods that monitor fluorescent properties of artificially introduced probes, the CARS approach directly addresses the H_2O/D_2O molecules, thereby circumventing complicated and possibly harmful labeling protocols. We have compared the CARS results with the method based on the fluorescence isotope effect of the ANTS fluorophore as a contrast agent for tracking water efflux (24). Contrary to earlier studies, here we apply the fluorescence method to single living cells. The fluorescent probe was excited with 636-nm radiation from the OPO under the same conditions as in the CARS experiment. The fluorescence quantum yield of the ANTS probe shows a 4-fold increase when the solvent is changed from H_2O to D_2O. The sensitivity of the probe is reflected in the TPE fluorescence lifetime dependence on different volume mixtures of H_2O/D_2O (Fig. 6*c Inset*). When axenic *D. discoideum* cells are incubated with a buffered solution of ANTS, the fluorophore is encapsulated in cytosolic vesicles. In Fig. 6*b*, the fluorescence lifetime image of a labeled cell in aqueous buffer is shown. The average fluorescence lifetime is 4.5 ns, which is consistent with the aqueous environment of the probe molecules. In Fig. 6*c*, the results of a transient flushing experiment are depicted. As is evident from the figure, the change in the TPE fluorescence lifetime during the water efflux yields traces isomorphic to the CARS signal that was measured simultaneously. In retrospect, the CARS results validate the assumption previously made that the ANTS probe presents an inert probe for water diffusion measurements. Nevertheless, spatial variations in the water concentration are difficult to map in the intracellular domain by using fluorescence techniques, as a result of incomplete homogeneous staining. Active exclusion of the chromophores from the aqueous cytosolic region and accumulation of the dye in specific organelles usually hinder uniform fluorescent staining of the interior of the cell. Moreover, the

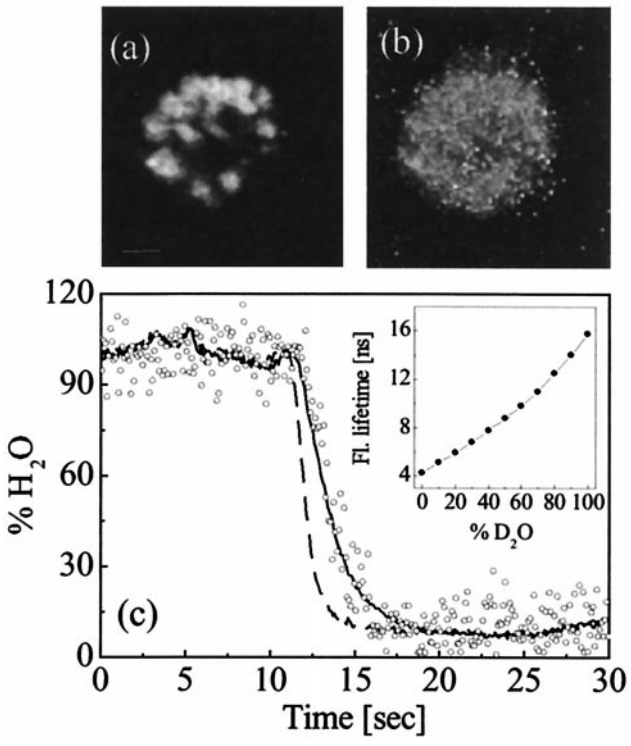

Fig. 6. TPE fluorescence of *D. discoideum* that have been labeled with ANTS. (*a*) TPE fluorescence intensity image. Fluorescent probe is accumulated in cytosolic vesicles. (Bar = 2 μm.) (*b*) Fluorescence lifetime image of the same cell. Average lifetime is determined to be 4.5 ns, corresponding to an aqueous environment. (*c*) Simultaneous measurement of total intracellular CARS signal (solid line) and lifetime change of the ANTS fluorophore (dots) during a flushing event. Dashed line indicates the response time of the perfusion chamber. *Inset* shows the change in TPE fluorescence lifetime of a 10 mM ANTS solution for different volume fractions of D_2O relative to H_2O.

unspecific binding of fluorescent probes to intracellular compounds will hamper reliable diffusion measurements.

Conclusions

The application of the CARS method to the study of intracellular hydrodynamics offers a unique approach to the determination of biophysical transport parameters. The high CARS signal yield obtained from intracellular water has permitted us to perform dynamical measurements by monitoring the H_2O/D_2O exchange in living cells. Excellent morphological contrast is obtained in small cells such as *D. discoideum* that measure only 10 μm in diameter. Contrary to NMR methods, intracellular water domains can be separated clearly from the extracellular environment, and regions of severely restricted water mobility may be readily identified within the cell. Comparison with fluorescence techniques reveals that the spatial mapping of the intracellular water diffusion coefficient is a unique feature of the CARS microscope that cannot be realized by using analogous fluorescence methods. The CARS method is intrinsically limited by the finite response time of the perfusion chamber, which is currently set by the maximum allowable shear force that the cells can handle. As a consequence, fast cellular efflux rates may not be resolved on the time scale of the experiment. For a 10-μm-sized cell, diffusion membrane permeability constants up to 50 μm/s may still be accurately measured with a perfusion chamber time constant of 1.5 s. The maximum detectable P_d scales roughly linear with the cell size, implying that the method becomes more sensitive for larger-sized cells. Improvement of instrument design and detection sensitivity may ultimately lead to the real-time two-dimensional (x, y) mapping of water efflux in living cells, providing a direct means for recognizing local intracellular regions of restricted water mobility. The experiments with *D. discoideum* cells presented establish that it is possible to track intracellular hydrodynamics at a single-cell level and to correlate the measured effusion patterns to biophysical parameters that characterize restricted water diffusion and permeability. The all-optical microscopic approach will be a valuable tool in quantitative physiological studies providing insight in biophysical transport phenomena in relation to cellular structure and morphology not only at the single-cell level but also in larger multicellular assemblies.

Appendix

Intracellular water concentration is a function of both space and time. To model intracellular water diffusion, the cell is described by a membrane-bound half sphere with radius b. Diffusion is considered along the radial coordinate r. The interior of the cell is divided in two compartments: close to the plasma membrane, water mobility is characterized by a low diffusion constant D_{low} ($a < r < b$), whereas the central part of the cell is described by a high diffusion coefficient D_{high} ($0 < r < a$). Under the assumption that $D_{\text{high}} \gg D_{\text{low}}$, the water concentration is described by the diffusion equation:

$$\frac{\partial c(r,t)}{\partial t} = D_{low}\frac{\partial^2 c(r,t)}{\partial r^2} \quad \text{at } a < r < b$$

$$c(r,t) = c(a,t) \quad \text{at } 0 < r < a$$

with boundary conditions:

$$\frac{\partial c(r,t)}{\partial r} = 0 \quad \text{at } r = a$$

$$D_{low}\frac{\partial c(r,t)}{\partial r} + P_d\, c(r,t) = 0 \quad \text{at } r = b$$

The solution of this set of equations is given by ref. 25:

$$c(r,t) = \frac{2}{r}\sum_{n=1}^{\infty} \exp(-D_{low}\alpha_n^2 t) R_n(r)\left\{\frac{a-b}{\alpha_n}\cos[\alpha_n(b-a)] + \left(\frac{1}{\alpha_n} + ab\right)\sin[\alpha_n(b-a)]\right\}$$

where $R_n(r)$ is defined as:

$$\frac{(bh-1)^2 + b^2\alpha_n^2}{q_n}\{\sin(r-a)\alpha_n + a\alpha_n\cos(r-a)\alpha_n\}$$

and

$$q_n = (b-a)(a^2\alpha_n^2 + 1)\{b^2\alpha_n^2 + (bh-1)^2\} + \{a(bh-1) + b\}(bh - 1 + ab\alpha_n^2)\,.$$

Here $h = P_d/D_{low}$, and α_n is given by the roots of the equation

$$\{(bh-1) - ab\alpha^2\}\sin(b-a)\alpha + \alpha\{a(bh-1) + b\}\cos(b-a)\alpha = 0$$

Experimental traces are simulated by convolving the calculated concentration pattern with the measured response function of the perfusion chamber.

We thank W.F. Loomis (University of California, San Diego) for the generous supply of aquaporin-transformed act15::rd28 cells. L. Bosgraaf and J. Roelofs are greatly acknowledged for their help in culturing the cells and E. Boekema for his help in the image analysis. The software written by F. de Haan has been indispensable in this work.

1. Lodish, H., Berk, A., Lawrence Zipursky, S., Matsudaira, P., Baltimore, D. & Darnell, J. E. (1999) *Molecular Cell Biology* (Freeman, New York).
2. Finkelstein, A. (1987) *Water Movement Through Lipid Bilayers, Pores and Membranes* (Wiley, New York).
3. Crick, F. (1970) *Nature (London)* **225,** 420–422.
4. Huster, D., Jin, A. J., Arnold, K. & Gawrisch, K. (1997) *Biophys. J.* **73,** 855–864.
5. Reginald Waldeck, A., Hossein Nouri-Sorkhabi, M., Sullivan, D. R. & Huchel, P. W. (1995) *Biophys. Chem.* **55,** 197–208.
6. Ye, R. G. & Verkman, A. S. (1989) *Biochemistry* **28,** 824–829.
7. Pfeuffer, J., Flogel, U., Dreher, W. & Leibfritz, D. (1998) *NMR Biomed.* **11,** 19–31.
8. Gulani, V., Iwamoto, G. A. & Lauterbur, P. C. (1999) *Magn. Reson. Med.* **41,** 241–246.
9. Duncan, M. D., Reintjes, J. & Manuccia, T. J. (1982) *Opt. Lett.* **7,** 350–352.
10. Zumbusch, A., Holtom, G. R. & Xie, X. S. (1999) *Phys. Rev. Lett.* **82,** 4142–4145.
11. Müller, M., Squier, J., de Lange, C. A. & Brakenhoff, G. J. (2000) *J. Microsc. (Oxford)* **197,** 150–158.
12. Eesley, G. L. (1981) *Coherent Raman Spectroscopy* (Pergamon, New York).
13. Levenson, M. D. & Kano, S. S. (1987) *Introduction to Nonlinear Laser Spectroscopy* (Academic, San Diego).
14. Potma, E. O., de Boeij, W. P., Pshenichnikov, M. S. & Wiersma, D. A. (1998) *Opt. Lett.* **23,** 1763–1765.
15. Denk, W., Strickler, J. H. &. Webb W. W. (1990) *Science* **248,** 73–76.
16. Draaijer, A., Sanders, R. & Gerritsen, H. C. (1995) in *Handbook of Biological Confocal Microscopy*, ed. Pawley, J. (Plenum, New York), p. 491.
17. Assaf, Y. & Cohen, Y. (2000) *Magn. Reson. Med.* **43,** 191–199.
18. Watanabe, T., Ohtsuka, A., Murase, N., Barth, P. & Gersonde, K. (1996) *Magn. Reson. Med.* **35,** 697–705.
19. Neujahr, R., Heizer, C., Albrecht, R., Ecke, M., Schwartz, J. M., Weber, I. & Gerisch, G. (1997) *J. Cell. Biol*. **139,** 1793–1804.
20. Kuwayama, H., Ecke, M., Gerisch, G. & van Haastert, P. J. M. (1996) *Science* **271,** 207–209.
21. Weeks, G. & Herring, F. G. (1980) *J. Lipid Res.* **21,** 681–686.
22. Flick, K. M., Shaulsky, G. & Loomis, W. F. (1997) *Gene* **195,** 127–130.
23. Chaumont, F., Loomis, W. F. & Chrispeels, M. J. (1997) *Proc. Natl. Acad. Sci. USA* **94,** 6202–6209.
24. Kuwahara, M. & Verkman, A. S. (1988) *Biophys. J.* **54,** 587–593.
25. Carslaw, H. S. & Jaeger, J. C. (1959) in *Conduction of Heat in Solids* (Oxford Univ. Press, London), 2nd Ed., p. 237.